Structural transformation and vibrational properties of BaO_2 at high pressures

I. Efthimiopoulos,[1] K. Kunc,[1,*] S. Karmakar,[1] K. Syassen,[1] M. Hanfland,[2] and G. Vajenine[1,3,†]
[1]*Max-Planck-Institut für Festkörperforschung, Heisenbergstraße 1, D-70569 Stuttgart, Germany*
[2]*European Synchrotron Radiation Facility, F-38043 Grenoble, France*
[3]*Institut für Anorganische Chemie, Universität Stuttgart, Pfaffenwaldring 55, D-70569 Stuttgart, Germany*
(Received 24 July 2010; revised manuscript received 29 September 2010; published 28 October 2010)

The tetragonal ambient-pressure phase of BaO_2 (CaC_2-type, space group $I4/mmm$) with sixfold coordination of Ba atoms and O_2 dumbbells was found to transform reversibly to an orthorhombic modification (space group *Cmmm*) near 33 GPa. The eight-coordinated high-pressure phase represents a new structure type. It is related to the CsCl-type structure but can also be viewed as a distorted variant of the hexagonal AlB_2 type, suggesting possible polymerization of the isolated O_2 dumbbells to a two-dimensional network at higher pressure. In addition to *in situ* x-ray diffraction, Raman measurements were performed to study the lattice dynamics of the BaO_2 phases under pressure. The experimental observations are compared to the results of *ab initio* calculations of the structural stability and dynamical properties. Raman spectra of barium monoxide BaO are reported in the Appendix; these results were found useful for the interpretation of the Raman scattering of BaO_2.

DOI: 10.1103/PhysRevB.82.134125 PACS number(s): 62.50.−p, 64.70.kp, 71.15.Nc, 78.30.Am

I. INTRODUCTION

Inorganic peroxides of monovalent ($M^{I}_2O_2$ with M^{I}=Li-Cs) and divalent ($M^{II}O_2$ with M^{II}=Mg-Ba and Zn-Hg) metals[1] are some of the typical examples of ionic compounds containing a polyanion, in this case a peroxide $[O\text{-}O]^{2-}$ group with a closed-shell electronic configuration. The peroxide anion here can be viewed according to the Zintl concept:[2] the full transfer of the metal valence electrons to the nonmetal atoms leads to seven valence electrons per oxygen atom, leading to a formation of a single bond between them in the peroxide anion in accordance with the octet rule, similar to the isoelectronic neutral dihalogen molecules.

The first synthesized peroxide was BaO_2, obtained by Alexander von Humboldt[3] in 1799 from barium oxide BaO and air. Having been a practical source of hydrogen peroxide in the early days, its oxidizing properties due to oxygen release are still used. Since the discovery of the barium-containing superconductors on the oxocuprate basis, BaO_2 was investigated with renewed interest as a promising starting material.[4]

The first structural report on SrO_2 and BaO_2 dates back to 1935.[5] Further studies on BaO_2 confirmed the presence of a single bond between the oxygen atoms by accurately determining its length by x-ray diffraction on powder[6] and single crystals[4] (1.49 Å), as well as by measuring the Raman frequency corresponding to the stretching of the peroxide group[7] (842 cm^{-1}).

The crystal structure of BaO_2 can be viewed as a derivative of the cubic NaCl (B1) structure type: while the Ba atoms occupy the sodium sites, the centers of mass of the peroxide groups correspond to the chlorine positions. All O_2 dumbbells lie parallel to each other, pointing toward two barium atoms of the surrounding octahedron. Such local anisotropy in the coordination environment leads to an elongation of the octahedron and to a tetragonal distortion of the overall structure. The resulting body-centered tetragonal structure of the CaC_2 type[8] is the most common arrangement observed for $A[B_2]$ compounds containing covalently bound B_2 dumbbells (Fig. 1, left).

While temperature-induced structural transformations have been observed for several $A[B_2]$ compounds (such as identification of four different phases for CaC_2 itself,[9] for example), to our knowledge only two pressure-induced structural transformation have been identified, the CaC_2-type to hexagonal transition of UC_2 (Ref. 10) and the CaC_2-type to ThC_2-type phase change in LaC_2.[11,12]

BaO_2 was chosen as a test substance for a high-pressure study with an expectation of structural transformations occurring at relatively low pressures due to the presence of a heavy element, barium. The aim of this study was threefold: investigation of the evolution of the crystal structure and

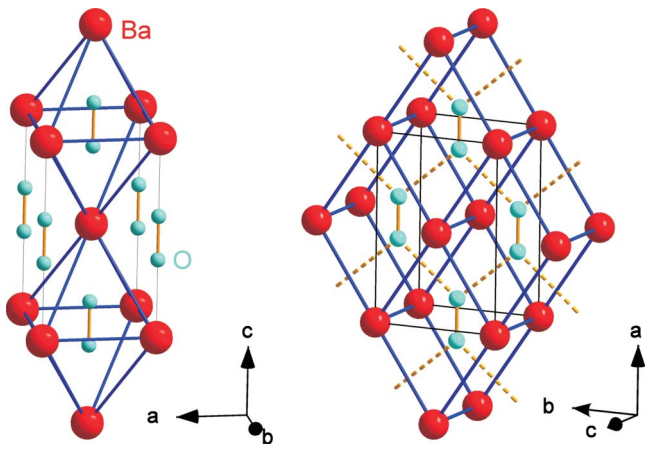

FIG. 1. (Color online) Left: crystal structure of the ambient-pressure tetragonal phase (space group $I/4mmm$, Z=2) of BaO_2. The large (red) and small (cyan) spheres correspond to Ba and O atoms, respectively. In this structure, the Ba atoms form an octahedral environment around the O_2 dumbbells. Right: crystal structure of the high-pressure orthorhombic phase (space group *Cmmm*, Z=2) of BaO_2. In this structure, the Ba atoms form a distorted cube around the O_2 dumbbells. The dashed lines indicate the next-nearest-neighbor contacts between the oxygen atoms and emphasize the relationship to the AlB_2 structure type.

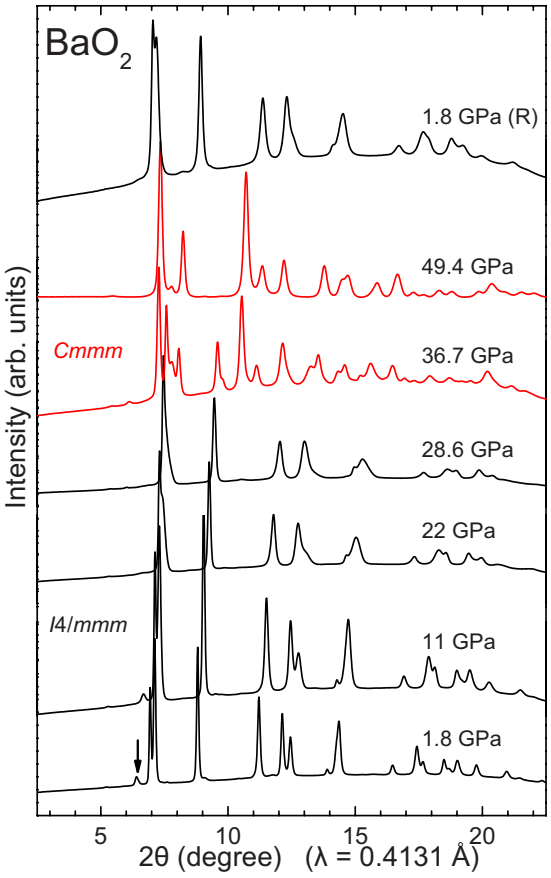

FIG. 2. (Color online) X-ray diffraction patterns of BaO_2 at selected pressures (λ=0.4131 Å, T=300 K). The arrow denotes the strongest diffraction maximum of the $BaCO_3$ impurity phase.

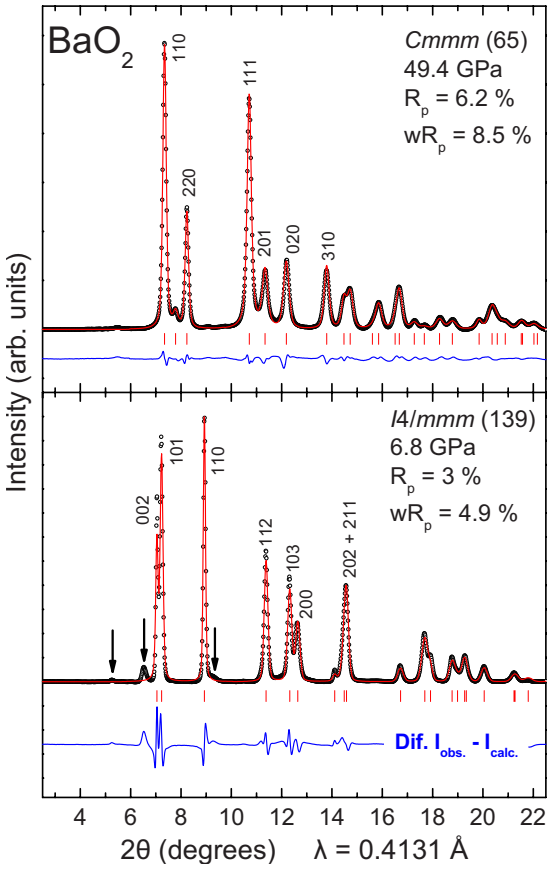

FIG. 3. (Color online) Refined XRD patterns of BaO_2 at 6.8 GPa (bottom, $I/4mmm$) and at 49.4 GPa (top, *Cmmm*). Circles correspond to the measured profile, the solid lines drawn through data represent the results of Rietveld refinements. The difference curves are shown also. Vertical ticks mark Bragg peak positions. The arrows point to the strongest diffraction peaks of the $BaCO_3$ impurity phase.

vibrational spectra as a function of pressure within the ambient-pressure CaC_2-type modification, identification of high-pressure phases, and answering the question whether the peroxide group is stable under high pressure.

II. EXPERIMENTAL AND COMPUTATIONAL DETAILS

BaO_2 polycrystalline powder (Merck, ≥93%) was handled under argon atmosphere in order to avoid reactions with moisture and carbon dioxide from the air. An x-ray diffraction (XRD) pattern measured at ambient pressure on BaO_2 sealed in a glass capillary (STOE STADI-P diffractometer with Cu $K\alpha_1$ radiation) was indexed with a tetragonal body-centered unit cell based on the positions of 17 diffraction maxima yielding a=3.8118(2) Å and c=6.8476(6) Å (V_{cell}=99.494 Å^3). These unit cell parameters are in a very good agreement with previous results reported for powders[6] and single crystals[4] and are consistent with the BaO_2 stoichiometry.[13] Additional weak diffraction maxima were assigned to the witherite-type $BaCO_3$ impurity.

In situ high-pressure diffraction experiments were conducted at room temperature with a gasketed diamond anvil cell (DAC). Pressures were measured by the well-established ruby luminescence method.[14] Silicone oil was employed as pressure-transmitting medium (PTM). Diffraction data were collected at the ID09A beamline of the European Synchrotron Radiation Facility, Grenoble, using a MAR555 flat panel detector. The monochromatic x-ray beam (wavelength λ =0.4131 Å) was collimated to a nominal diameter of 30 μm. In order to improve powder averaging, the DAC was rocked by ±3°. The scanned two-dimensional diffraction patterns were corrected for tilt and scanner distortions and converted to intensity vs 2θ data using the FIT2D software.[15] Rietveld refinements of the crystal structures were performed using the GSAS program.[16]

In situ Raman spectra were recorded at room temperature with a microscope laser Raman system (Jobin-Yvon, LabRam) operating with excitation lines λ=632.82 nm and λ =532 nm at 1 mW. Whereas pressure was controlled by the ruby luminescence method as well, no PTM was employed in order to avoid possible interference from its luminescence and reaction at the sample surface.

The calculations presented here were carried out according to the methodology described earlier, e.g., in Refs. 17 and 18: within the framework of the density-functional theory (DFT) in the generalized gradient approximation (GGA) (Ref. 19) with a plane-wave basis set and projector augmented waves (PAW) potentials[20] using the vasp codes.[21] The $5s^2$, $5p^6$, and $6s^2$ states of barium were treated as va-

lence states (i.e., ten electrons are dealt with explicitly; PAW-potential labeled as Ba_sv) while the potential denoted in the database[21] as O_h (h="hard") was chosen for oxygen. The plane-wave cutoff E_{pw}=875 eV was used and the *k*-point sampling of the reciprocal space was performed on $4\times4\times4$ meshes of the Monkhorst-Pack type[22] (11 and 12 irreducible *k* points for tetragonal and orthorhombic structures, respectively). Insulating behavior was assumed and confirmed for both phases throughout the studied pressure range. The calculations on both structures were carried out based on the periodicity defined by the respective primitive unit cells containing one formula unit BaO_2 each. For each crystal volume the ratios of the unit cell parameters and the free internal atomic parameter of the oxygen atom were optimized with respect to the total energy. Pressure *P* was evaluated directly from the DFT with the aid of stress theorem.[23]

III. STRUCTURAL PROPERTIES UNDER PRESSURE

At ambient conditions, BaO_2 crystallizes in the tetragonal CaC_2-type structure (space group $I4/mmm$, Z=2, Fig. 1, left). The structure can be described as a tetragonally distorted NaCl-type arrangement, with Ba atoms on the Na site, and O_2 dumbbells occupying the Cl site. With all peroxide units parallel to the *c* axis, the coordination octahedron is elongated.

A selection of typical XRD patterns at various pressures is shown in Fig. 2. The strongest diffraction maximum of the impurity phase $BaCO_3$ (marked by an arrow in Fig. 2) was present from the beginning up to about 15 GPa which exceeds a bit the reported upper pressure limit for observing its witherite modification.[24,25] The tetragonal CaC_2-type phase of BaO_2 is stable up to 33.6 GPa. At that pressure, clear signs of a pressure-induced structural transition are observed with the appearance of additional Bragg peaks corresponding to a high-pressure phase. Diffraction maxima of both phases were observed up to 45 GPa with only the high-pressure phase present above this pressure and up to the highest pressure of 49.4 GPa employed in this study. The new diffraction peaks could be indexed with an orthorhombic unit cell (space group *Cmmm*, Z=2). Upon pressure release, the ambient-pressure $I4/mmm$ phase was recovered (Fig. 2). Compared to the starting conditions, the diagram of the back-transformed sample is broadened and shows some differences in intensities which are presumably caused by grain size effects and some preferred orientation, respectively.

Representative Rietveld refinements for the $I4/mmm$ and *Cmmm* phases are shown in Fig. 3 for the patterns collected at 6.8 GPa and 49.4 GPa, respectively. The corresponding structural details are summarized in Table I.

The orthorhombic structure of BaO_2 features eightfold coordination of the peroxide groups, still all aligned parallel to each other, by the Ba atoms in form of distorted cubes related to the CsCl (B2) archetype (Fig. 1, right). While most $A[B_2]$ compounds crystallize in NaCl-related structures, the orthorhombic BaO_2 not only represents a new structure type, but is also just the second example of the CsCl-related arrangement for such compounds, in addition to the tetragonal SrS_2 structure type.[26,27] Thus the observed pressure-induced tetragonal-to-orthorhombic phase transition in BaO_2 can be simplistically viewed as being related to the NaCl-to-CsCl-type transformations common for ionic *AB* compounds under pressure.

TABLE I. Refined crystallographic data at two different pressures for the ambient-pressure tetragonal and the high-pressure orthorhombic modifications of BaO_2. The crystal volumes *V* refer to the *conventional* unit cells. The site notation follows Wyckoff, residuals *R* as defined in GSAS (Ref. 16).

	Tetragonal	Orthorhombic
Space group	$I4/mmm$ (139)	*Cmmm* (65)
Pressure (GPa)	6.8	49.4
a (Å)	3.7524(1)	5.7551(4)
b (Å)	3.7524(1)	3.8922(2)
c (Å)	6.7287(1)	3.0424(3)
V (Å^3)	94.74(3)	68.15(1)
Z	2	2
R_p, wR_p	0.03, 0.049	0.062, 0.085
Ba site	2*a* (0,0,0)	2*a* (0,0,0)
O site	4*e* (0.5,0.5,*z*)	4*h* (*x*,0,0.5)
	z=0.1055(12)	*x*=0.3768(15)
O-O bond length (Å)	1.445(7)	1.418(12)

At 49.4 GPa, the secondary O···O contacts between the peroxide groups (marked with dashed lines in Fig. 1, right) are found to be still significantly longer (2.43 Å) than the short O-O distances within the dumbbells (1.42 Å) but they are substantially shorter than the analogous secondary contacts in the tetragonal phase at ambient pressure (3.31 Å). Hence, the high-pressure orthorhombic modification of BaO_2 can be viewed as the first step toward a polymerization of the peroxide groups. One could speculate that a further shortening of these secondary contacts in the *Cmmm* phase of BaO_2 might lead to a more symmetrical graphitelike sheet of oxygen atoms at higher pressures with the hexagonal AlB_2-type structure being a possible structure candidate. Polymerization of oxygen in BaO_2 would lead to metallization.

Recalling the analogy between the peroxide anion and neutral dihalogen molecules, a parallel between pressure-induced metallization of elemental halogens and polymerization of the peroxide groups in BaO_2 could be envisioned. Since elementary fluorine is likely to turn metallic at a pressure significantly higher compared with the heavier halogens, it could be hypothesized that the isolelectronic peroxide anion in BaO_2 is likely to polymerize and thus metallize way beyond a pressure of 100 GPa. However, pressure-induced metallization by a different process, i.e., the closing of the band gap between oxygen-derived valence band states and the predominantly 5*d* conduction-band states of barium, is perhaps more likely. For the discussion of pressure-induced metallization by band closing in the related barium monochalcogenides (including BaO) see, e.g., Refs. 28–31. As a consequence of a smaller optical gap,[32] BaO_2 can be assumed to turn metallic at a pressure lower than BaO.

The pressure variations in the crystal volume and structural parameters for BaO_2 in the low- and high-pressure

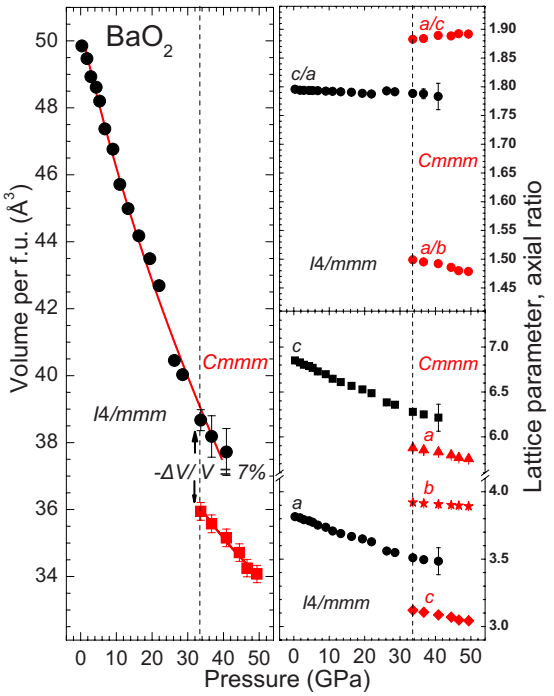

FIG. 4. (Color online) Volume per formula unit, axial ratios, and lattice parameters for the low- and high-pressure phases of BaO_2. Solid lines represent guides to the eye. The dashed lines mark the onset of the structural transition.

phases are shown in Fig. 4. Taking the PV data for the tetragonal $I4/mmm$ phase up to 20 GPa and using a Rydberg-Vinet equation of state[33] (EOS), we obtain

$$V_0 = 50.3(3)\ \text{Å}^3, \quad B_0 = 105(20)\ \text{GPa}, \quad B_0' = 3(2).$$

The standard deviations for bulk modulus $B_0 = -(VdP/dV)_0$ and its pressure derivative $B_0' = (dB/dP)_0$ (index zero for zero pressure) are large. This we attribute in part to the nonhydrostatic nature of the pressure conditions. The first-order transformation to the high-pressure $Cmmm$ phase is accompanied by a relative volume decrease of

$$\frac{\Delta V}{V} = -0.07(1).$$

The PV data for the $Cmmm$ phase, approximated by a Rydberg-Vinet EOS give

$$V_T = 36.00(13)\ \text{Å}^3, \quad B_T = 259(25)\ \text{GPa}$$

at the reference pressure $P_T = 33.6$ GPa ($B_T' = 3$ fixed).

IV. HIGH-PRESSURE RAMAN RESULTS

Raman spectra of BaO_2 are shown in Fig. 5(a), the frequencies of Raman features are plotted in Fig. 5(b) as a function of pressure and quantitative information on the effect of pressure on Raman mode frequencies of BaO_2 is collected in Table II.

For the ambient-pressure tetragonal phase $I4/mmm$ two first-order Raman modes are expected, having E_g and A_{1g} symmetry.[34,35] The low-frequency E_g mode is twofold degenerate and corresponds to the librational motion of the O_2 units. The high-frequency A_{1g} mode is a stretching motion of the peroxide group. These two modes are observed in the zero-pressure Raman spectra at 202 cm^{-1} and 843 cm^{-1}, respectively. The A_{1g} mode dominates the spectrum, the E_g mode is much weaker, cf. Fig. 5(a). Other weak Raman features are seen at low pressures [asterisks in Fig. 5(a)]. These can be attributed to the presence of the $BaCO_3$ impurity.[24] The impurity features fade out with increasing pressure which is attributed to a sluggish structural phase transition of $BaCO_3$ under pressure.[24,25]

Upon pressure increase, two major changes of the Raman spectra are observed at about 14 GPa and at 30 GPa, respectively. The changes at 30 GPa are attributed to the tetragonal-to-orthorhombic structural transition, in accordance with the results of the XRD study. For the orthorhombic $Cmmm$ phase, three Raman modes are expected (see theoretical results below as well): two low-frequency modes of B_{1g} and B_{2g} symmetries, and a higher lying A_{1g} mode. Like in tetragonal BaO_2, the A_{1g} mode corresponds to the O-O stretching motion. It appears at frequencies higher than that of the respective A_{1g} mode of the tetragonal phase and exhibits a similar shift with pressure, see Figs. 5(a) and 5(b). The B_{1g} and B_{2g} modes correspond to O_2 librations, similar to the E_g mode in the tetragonal phase but with degeneracy removed. While the frequency of the B_{1g} mode increases with pressure, the B_{2g} mode tends to soften, see Fig. 5(b).

The two Raman features D_1 and D_2 that appear in the 400–600 cm^{-1} frequency range above 14 GPa were first thought to originate from impurity phases such as $BaCO_3$ and possibly BaO. However, $BaCO_3$ shows no Raman modes in this frequency region.[24] Also, no structural phase transition is known for $BaCO_3$ in the vicinity of 15 GPa.[25] As for BaO, it undergoes structural changes at pressures of 10 GPa and 15 GPa.[36] Since the corresponding Raman spectra have not been reported, we have investigated the effect of pressure on the Raman scattering of BaO. The details are given in the

TABLE II. Assignment (Refs. 34 and 35), frequencies, pressure coefficients, and mode Grüneisen parameters γ of the Raman modes of BaO_2. The mode frequencies and their slopes refer to reference pressures of $P_r = 0$ GPa, 14 GPa, and 30 GPa for the $I4/mmm$ phase, the unidentified modes in that phase, and the $Cmmm$ phase. The linear pressure coefficients $\partial\omega/\partial P$ were obtained by quadratic fits to the measured data. The values of the mode Grüneisen parameters γ are obtained using $\gamma = (B/\omega)(\partial\omega/\partial P)$, where $B = 105$ GPa for the $I4/mmm$ phase and $B = 250$ GPa for the high-pressure $Cmmm$ phase at 30 GPa.

Phase	Mode	ω_r (cm^{-1})	$\partial\omega/\partial P$ (cm^{-1}/GPa)	γ
$I4/mmm$	E_g	202	7.7	4.0
$P_r = 0$ GPa	A_{1g}	843	4.9	0.6
Unidentified	D_1	378	3.8	
$P_r = 14$ GPa	D_2	506	8.9	
$Cmmm$	B_{1g}	306	2.3	2.3
$P_r = 30$ GPa	B_{2g}	280	−0.2	−0.1
	A_{1g}	988	4.8	1.3

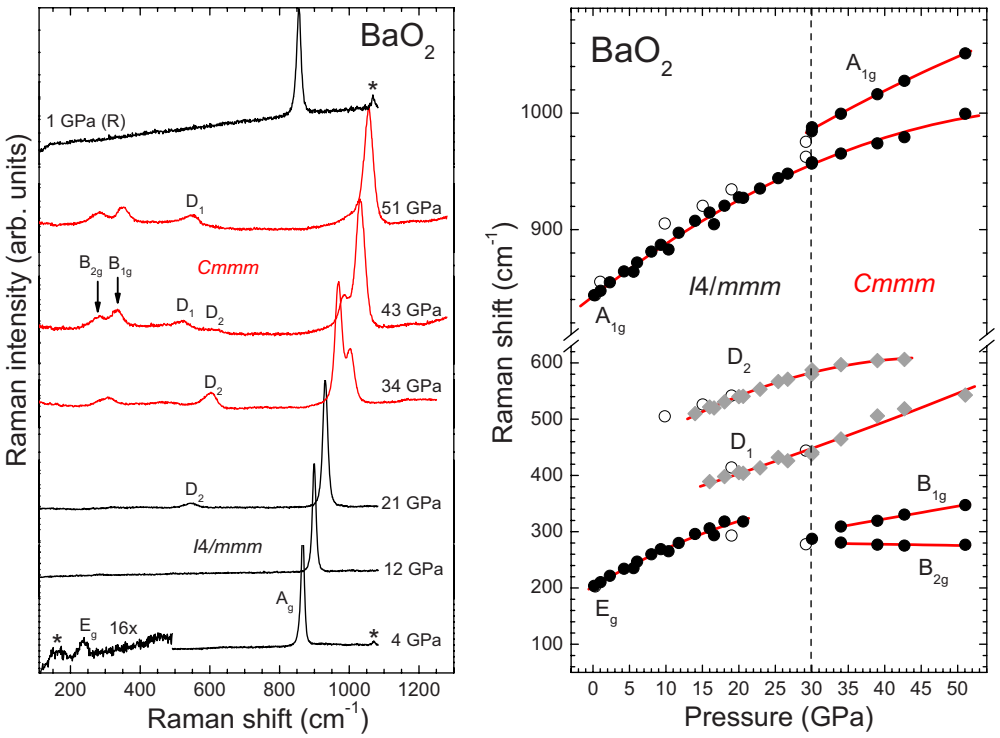

FIG. 5. (Color online) Left: Raman spectra of BaO_2 at various pressures. The laser excitation wavelength is $\lambda = 633$ nm. Spectra below 30 GPa correspond to the tetragonal phase. The asterisks denote weak Raman peaks assigned to the $BaCO_3$ impurity phase; they fade out with increasing pressure. The arrows indicate new Raman modes appearing as a result of the sluggish structural phase transition to the orthorhombic phase. The modes marked by D_1 and D_2, seen at pressures above 13 GPa, are tentatively assigned as defect modes (see text); they appear to exchange intensity with increasing pressure. Right: Frequencies of the observed Raman modes of BaO_2 as a function of pressure. Solid and open circles correspond to data measured for increasing and decreasing pressure, respectively. Diamonds refer to the D modes. Lines represent linear/quadratic relations fitted to the data. The vertical dashed line marks the onset of the structural phase transition as seen in the Raman scattering experiments.

Appendix. All of the Raman modes of BaO lie at frequencies lower than the D features seen for BaO_2 above 14 GPa. So, these modes cannot be attributed to a BaO impurity phase. All of the above make us believe that the extra Raman features that appear in Raman spectra above 14 GPa are intrinsic to the BaO_2 phase. They may originate from a local symmetry breaking which cannot be seen in x-ray diffraction, from defect-induced scattering, or from acoustic overtones. In other words, their assignment remains uncertain at this point.

V. COMPUTATIONAL RESULTS

The electronic structure of the tetragonal BaO_2 phase has been previously studied theoretically using the Hartree-Fock method[32,37] and density-functional theory.[38] According to these investigations the DFT achieves better performance, presumably due to the inclusion of the electronic correlation, which appears to be essential for the correct description of the localized bonding in the peroxide group.

A. Crystal structures of BaO_2 and their transformations

In order to test the structural stability of the considered structures with respect to possible distortions, the effect of the peroxide group rotations on the total energy was studied before the detailed structural calculations were undertaken. Small displacements in the b,c directions in the orthorhombic structure were probed, as well as in the a and a-b directions in the tetragonal structure. Three different magnitudes of the displacement ($u/b, u/c = 0.01$, 0.02, and 0.04 in the orthorhombic, $u/a = 0.02$, 0.04, and 0.06, as well as $0.02\sqrt{2}$, $0.04\sqrt{2}$, and $0.06\sqrt{2}$ in the tetragonal structure) and three different volumes ($V = 28$, 34, and 43 Å^3 per BaO_2 in the orthorhombic; 34, 40, and 49 Å^3 in the tetragonal structure) were tested. In all cases only *restoring* forces and *increase* in total energy were observed; no sign of any instability was found. We conclude that the O_2 dumbbells in the assumed orientation along the c axis in the tetragonal structure and along the a axis in the orthorhombic one correspond to the respective energy minima, at least to local ones. Large displacements (which would correspond, e.g., to the rotation of the peroxide groups by 90°) were not tested.

The computed $E(V)$ and $P(V)$ equations of state are shown in Fig. 6. These data were then converted into model EOS parameters reported in Table III. Both the calculated $E(V)$ and $P(V)$ data were used and the EOS parameters (equilibrium volume V_0, bulk modulus B_0, and pressure derivative B_0') quoted in Table III refer to the Holzapfel and Vinet model EOS which offered the best fits and/or the best consistency for the theoretical $E(V)$ and $P(V)$ data.

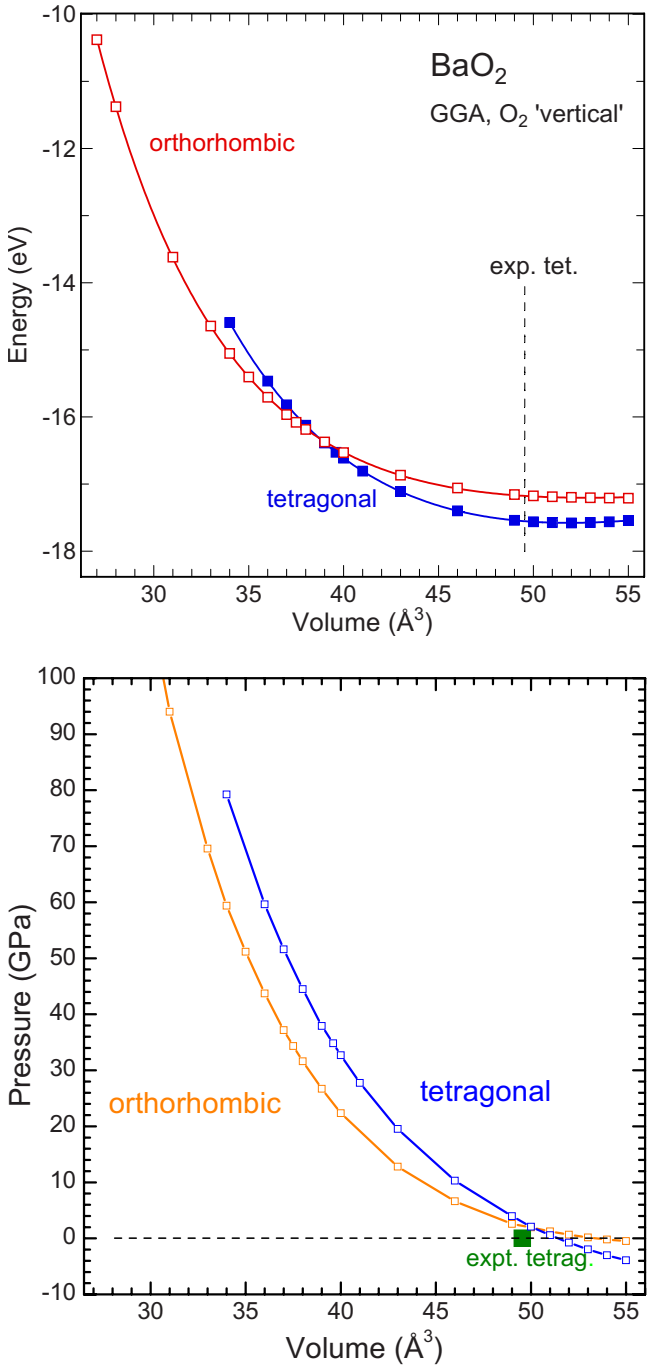

FIG. 6. (Color online) Calculated $E(V)$ and $P(V)$ equations of state for the tetragonal (solid squares) and orthorhombic (open squares) phases of BaO_2. The solid lines represent the fits of the respective Holzapfel or Vinet EOS expressions. Both volume and energy refer to one formula unit of BaO_2.

The two $E(V)$ equations of state intersect each other (Fig. 6) with the orthorhombic structure having lower energy at volumes below 39 Å^3. The calculation of the enthalpies situates the first-order tetragonal-to-orthorhombic transition at the pressure of P_T=34.2 GPa, accompanied by a volume contraction ΔV=−2.2 Å^3/BaO_2 (or −5.54%) from $V_{T,tet}$ =39.70 Å^3 to $V_{T,ortho}$=37.50 Å^3 (see Table IV), in a very good agreement with both XRD and Raman results.

TABLE III. The EOS parameters for the two phases of BaO_2 derived from calculated data. The least-squares fits to the calculated data by the Vinet (Ref. 33) and Holzapfel (Ref. 39) equations of state are based on 16 volumes in the interval 34.0–54.0 Å^3 per BaO_2 in the tetragonal structure, and on 21 volumes in the interval 27.0–55.0 Å^3 per BaO_2 in the orthorhombic phase. The uncertainties quoted correspond to 90% confidence range in the fitting procedure. All volumes V_0 refer to the *primitive* unit cells hosting one formula unit of BaO_2 each.

EOS model	Data	V_0 (Å^3)	B_0 (GPa)	B_0'
		Tetragonal		
Holzapfel	$E(V)$	51.88(2)	68.31(30)	4.97(2)
Holzapfel	$P(V)$	51.44(7)	70.04(90)	4.98(6)
		Orthorhombic		
Vinet	$E(V)$	53.08(46)	33.7(32)	6.61(22)
Vinet	$P(V)$	52.49(72)	36.5(40)	6.44(20)

The computed crystallographic data and their variation with volume are shown in Fig. 7: the lattice parameters, their ratios, the O-O distance within the peroxide group, and the two shortest Ba-O distances. The O-O distance is related to the only free internal parameters for the oxygen atoms: z in the tetragonal and x in the orthorhombic structure. These theoretical results are also in a reasonable agreement with the experimental data. Figure 7(d) illustrates that the shortest Ba-O distances increase at the phase transition, as is typical of pressure-driven NaCl-type to CsCl-type phase transitions.

B. Phonons in BaO_2

The structural transition reproduced by the calculations above is also reflected in the behavior of phonons. The frequencies of the Raman active modes were calculated using the "frozen-phonon" method.[40,41] The relevant modes in both structures are the O_2-bond stretching (A_{1g} in both modifications) or O_2-libration (E_g or B_{1g}, B_{2g}). The latter modes are doubly degenerate in the tetragonal structure (x,y directions equivalent) and split into two distinct modes when going over to the orthorhombic one (inequivalent b,c directions). We associate, arbitrarily, the indexing 1 and 2 of the B_g vibrations with, respectively, the b and c axes. Thus in B_{2g} the librations of the peroxide groups take place in the ac plane while in B_{1g} mode the librations are in the ab plane, within

TABLE IV. Quantities pertinent to the phase transition in BaO_2 as obtained from the present DFT-GGA calculations. All volumes are per one formula unit of BaO_2 (primitive unit cell).

	Tetragonal		Orthorhombic
$V_{P=0}$ (Å^3)	51.88		(53.08)
V_T (Å^3)	39.70		37.50
$\Delta V/V$		−5.54%	
P_T (GPa)		34.2	

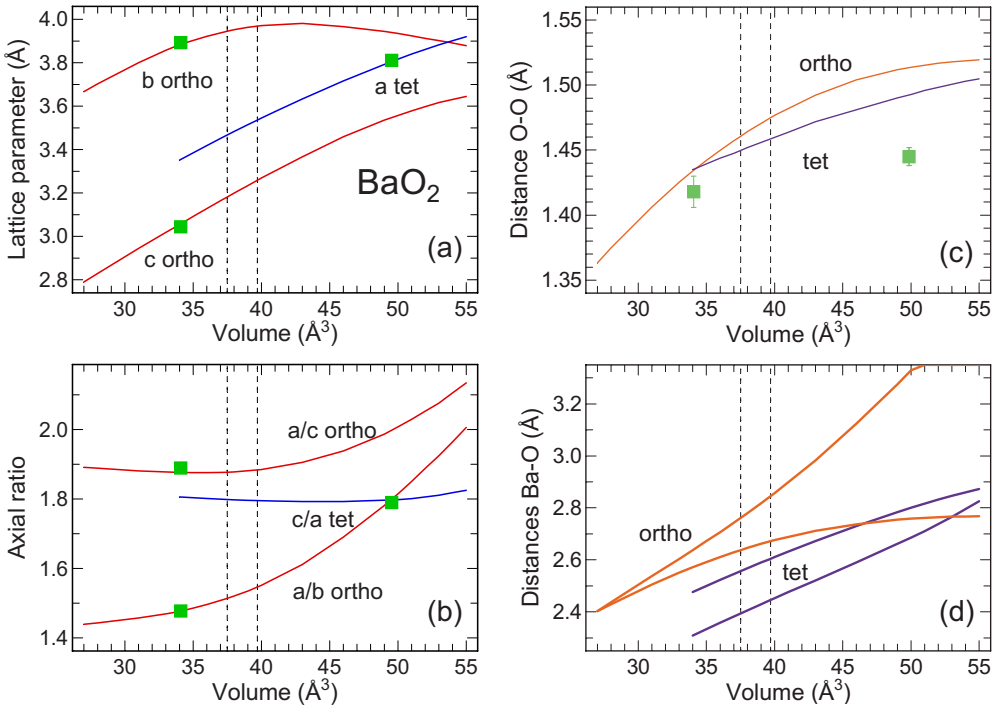

FIG. 7. (Color online) (a) Theoretically optimized lattice parameters, (b) axial ratios, (c) O-O distance, and Ba-O distances for the tetragonal and orthorhombic phases of BaO_2 as functions of volume per formula unit (solid lines) in comparison with the experimental results (filled squares) for the respective phases at 6.8 GPa ($I4/mmm$) and 49.4 GPa ($Cmmm$),cf. Table I. Vertical dashed lines mark the calculated volumes at the phase transition.

the pseudohexagonal two-dimensional network of the oxygen atoms.

In order to eliminate the cubic anharmonicity, we chose, at every volume, two A_{1g} displacement patterns—outward and inward—of magnitude $u/c=0.003$ and averaged the consequent increases in energy ΔE. The quartic anharmonicity was found to be negligible at this magnitude of u (error in frequency: $\approx 0.2\%$ at most). In the E_g modes the cubic anharmonicity is absent by symmetry but the quartic component is sizeable. Moreover, the displacements cannot be chosen too small because the modes turn out to have rather low frequency (meaning a small ΔE, where the computational errors might play a role). We thus chose, at every volume, five different displacements ranging from $u/a=0.01$ to $u/a=0.05$, fitted the calculated $\Delta E(u)$ by quartic polynomial, and retained the harmonic part. In the orthorhombic structure we proceeded similarly, choosing, again, $u/a=0.003$ for the A_{1g} displacement pattern and five magnitudes of u/b or u/c ranging from 0.01 to 0.05. The harmonic frequencies calculated for different volumes are shown in Fig. 8 for the two structures in comparison with the related experimental results. In all modes studied the relative anharmonicity (ΔE^{cubic} or $\Delta E^{\text{quartic}}$ with respect to the $\Delta E^{\text{harmonic}}$) was found to *decrease* with pressure.

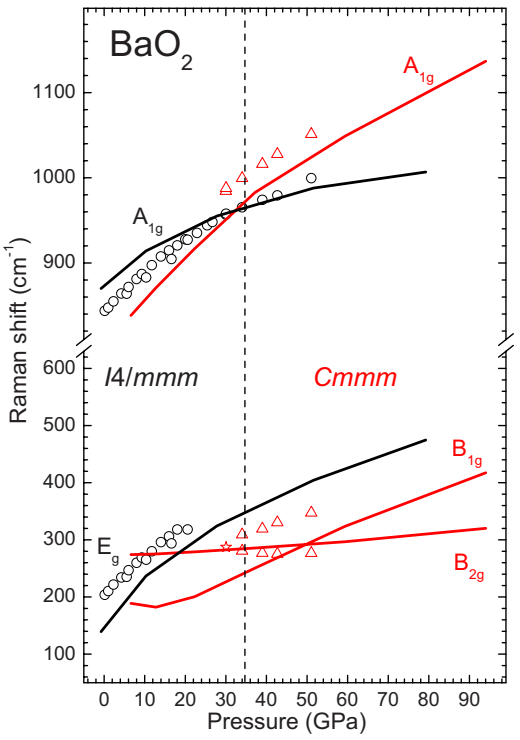

FIG. 8. (Color online) The theoretically calculated frequencies of Raman-allowed mode of BaO_2 for the tetragonal and orthorhombic modifications as a function of calculated pressure (solid lines). The dashed vertical line marks the calculated phase transition pressure. Measured Raman mode frequencies versus experimental pressure are shown by open symbols.

VI. DISCUSSION AND SUMMARY

Even though the crystal structure of the ambient-pressure tetragonal phase of BaO_2 contains covalently bonded peroxide anions all aligned parallel to the c axis, no substantial

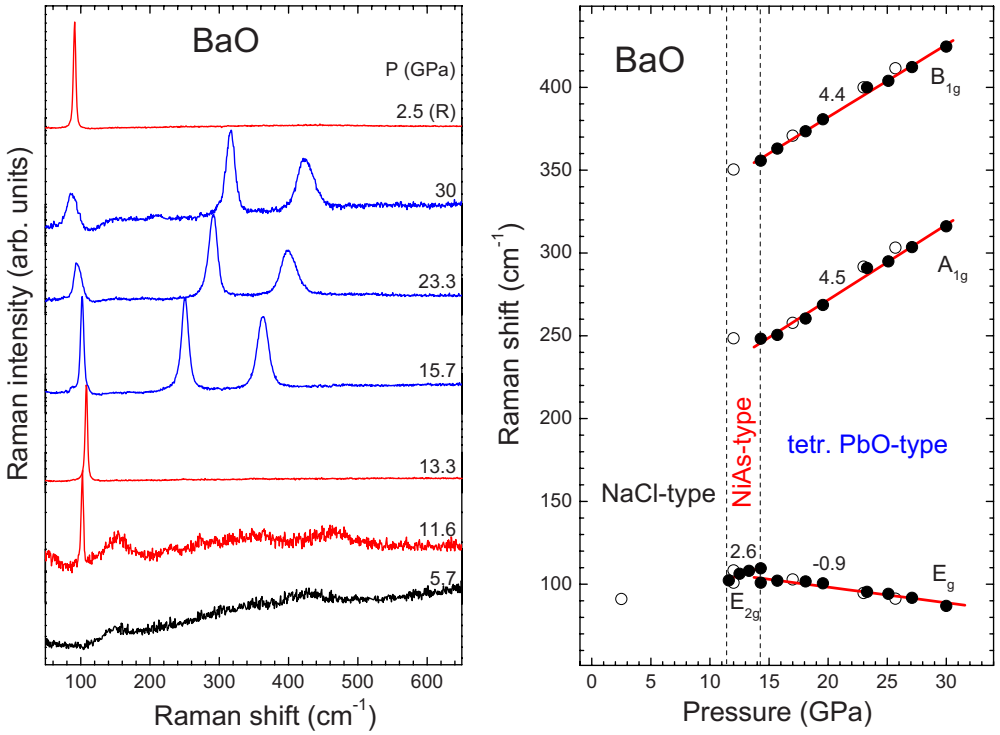

FIG. 9. (Color online) Left: Raman spectra of BaO measured at various pressures with $\lambda = 514.5$ nm excitation wavelength. Right: frequencies of the Raman modes of BaO as a function of pressure. Solid and open circles correspond to data measured for increasing and decreasing pressure, respectively. The pressures for structural phase transitions according to the present Raman study are indicated by vertical dashed lines. The pressure values agree with the earlier report of Weir *et al.* (Ref. 36). Numbers attached to the sets of data stand for pressure coefficients. The given mode assignment for tetragonal BaO-III is tentative.

anisotropy is observed regarding the compressibility under pressure. Both experimental (Fig. 4) and theoretical (Fig. 7) results agree on the fact that the c/a ratio remains nearly constant in the whole stability range of the tetragonal phase. Both Ba-O and O-O contacts shorten under pressure which is reflected by the parallel increase of the observed and computed A_{1g} and E_g vibrational frequencies, cf. Fig. 8. While the increase in the peroxide stretching frequency reflects shortening and stiffening of the O-O bond (also in agreement with the calculated evolution of the O-O bond length as a function of crystal volume, see Fig. 7), the increase in the libration frequency is a consequence of the shorter Ba-O contacts under pressure.

The reversible tetragonal-to-orthorhombic phase transition at high pressure follows the simple rule of the coordination number increase and parallels the classical NaCl-to-CsCl-type pressure-induced phase transitions known for the *AB* compounds. The orthorhombic phase crystallizes in a new structure type retaining the parallel orientation of the peroxide groups. Incidentally, the phase transition occurs near the volume where the phase with the shorter O-O distance is at the same time the more stable one (Fig. 7). The experimentally observed orthorhombic phase, its Raman spectrum and the evolution of Raman frequencies as a function of pressure are consistent with the computational results. This applies to the pressure dependence of the axial ratios (increase in b/a but almost no change in c/a with pressure, cf. Figs. 4 and 7) and the vibrational frequencies (increase for A_{1g} and B_{1g} but almost no change for B_{2g} with pressure, cf. Figs. 5 and 8). In addition, the phase transition parameters, such as the transition pressure, volume change, and the correspondence between the structural and vibrational parameters for the two phases could be well reproduced. Only the two newly appearing weak Raman modes in the medium frequency range cannot be attributed to the idealized structures considered and are likely to be due to local distortions.

The crystal structure of the high-pressure orthorhombic BaO_2 phase can be topologically related to the hexagonal AlB_2 structure type: the *Cmmm* phase can be viewed as a result of a pairing (Peierls) distortion in the two-dimensional graphitelike oxygen layer. This structural analogy suggests the possibility of a phase transition in BaO_2 to the AlB_2 type at even higher pressures, perhaps accompanied by metallization. Such a transition would need the b/a ratio for the *Cmmm* phase approaching the value of $1/\sqrt{3} = 0.577$; however, the experimentally observed b/a ratio is larger and increases as a function of pressure (Fig. 5). In addition, the analogy between isolectronic $[O\text{-}O]^{2-}$ and F_2 groups suggests that such metallization would take place at much higher pressures than the ones employed in this study.

ACKNOWLEDGMENTS

G.V.V. thanks Arndt Simon for the support during this study. The XRD work was carried out within the beam time allocated for the proposal HS 3933 at the European Synchrotron Radiation Facility (ESRF Grenoble). Part of this work benefited from access to the HPC resources of IDRIS under

the Allocation No. 2010-90208 made by GENCI (Grand Equipment National de Calcul Intensif).

APPENDIX: RAMAN SPECTRA OF BaO UNDER PRESSURE

Barium monoxide crystallizes in the NaCl-type structure. A transition toward the higher coordinated CsCl-type structure could be expected under pressure on the grounds of simple structural systematics of ionic *AX* compounds and in analogy to what is observed for BaO_2 in this study. However, BaO follows a more complex route under pressure.[36] The NaCl-type BaO-I transforms at 10 GPa to hexagonal NiAs-type BaO-II, followed by a transition at 15 GPa to tetragonal BaO-III. That phase is isostructural to the tetragonal litharge-type (red) PbO. The litharge BaO can be viewed as a distorted variant of the CsCl-type structure and indeed deforms toward CsCl at higher pressures.[36] Since no Raman data on the high-pressure modifications of BaO could be found in the literature, some Raman measurements were carried out in this work.

High-pressure Raman spectra of BaO are shown in Fig. 9. The spectra were measured using green laser excitation. Again, because BaO is hygroscopic, measurements were performed without using a pressure medium. Overall, the spectra indicate changes that appear to be fully consistent with the earlier structural study.[36] Below 10 GPa, Raman spectra are featureless as is expected for a NaCl-type phase. Some very weak and broad humps are seen that may originate from defect-induced scattering. BaO becomes Raman-active at about 11 GPa where it exhibits a single mode. This indicates the transition to the NiAs-type phase which indeed is expected to have only one Raman-active E_{2g} mode, which in this case is Ba related. At about 14 GPa, the Raman spectrum of BaO changes, now exhibiting three well-resolved Raman features of nearly comparable intensity.

Figure 9 also shows Raman frequencies of BaO as a function of pressure. Numbers attached to the data refer to average pressure coefficients. Within the figure, we indicate a tentative assignment of the Raman modes of BaO-III. This assignment follows from comparison with results for tetragonal PbO (Refs. 42 and 43) and isostructural SnO.[44] An interesting observation is that the low-lying E_g near 100 cm^{-1} (it corresponds to an in-plane vibration of the heavy Ba atoms) shows a softening with increasing pressure. This behavior may be related to approaching a structural instability. This aspect is left to further investigation.

The main point of interest in relation to the Raman spectra of BaO_2 is that all of the Raman modes of BaO lie at frequencies lower than those of the *D* modes observed in BaO_2 above 14 GPa.

*Permanent address: Physique des Milieux Denses, IMPMC, CNRS-UMR7590 and Université Pierre and Marie Curie, 140 rue de Lourmel, F-75015 Paris, France; karel.kunc@upmc.fr

†g.vajenine@fkf.mpg.de

[1] N.-G. Vannerberg, Prog. Inorg. Chem. **4**, 125 (1962).
[2] H. Schäfer, B. Eisenmann, and W. Müller, Angew. Chem. **85**, 742 (1973).
[3] A. v. Humboldt, *Versuche über die chemische Zerlegung des Luftkreises und über einige andere Gegenstände der Naturlehre* (Vieweg, Braunschweig, 1799), p. 130.
[4] W. Wong-Ng and R. S. Roth, Physica C **233**, 97 (1994).
[5] J. D. Bernal, E. Djatlowa, I. Kasarnowsky, S. Reichstein, and A. G. Ward, Z. Kristallogr. **92**, 344 (1935).
[6] S. C. Abrahams and J. Kalnajs, Acta Crystallogr. **7**, 838 (1954).
[7] H. H. Eysel and S. Thym, Z. Anorg. Allg. Chem. **411**, 97 (1975).
[8] M. v. Stackelberg, Z. Phys. Chem. B **9**, 437 (1930).
[9] M. Knapp and U. Ruschewitz, Chem.-Eur. J. **7**, 874 (2001).
[10] J.-P. Dancausse, S. Heathman, U. Benedict, L. Gerward, J. S. Olsen, and F. Hulliger, J. Alloys Compd. **191**, 309 (1993).
[11] X. Wang, I. Loa, K. Syassen, R. K. Kremer, A. Simon, M. Hanfland, and K. Ahn, Phys. Rev. B **72**, 064520 (2005).
[12] S. Karmakar, X. Wang, I. Efthimiopoulos, K. Syassen, V. Babizhetskyy, R. Kremer, and A. Simon (unpublished).
[13] M. Königstein, J. Solid State Chem. **147**, 478 (1999).
[14] H. K. Mao, J. Xu, and P. Bell, J. Geophys. Res. **91**, 4673 (1986).
[15] A. P. Hammersley, S. O. Svensson, M. Hanfland, A. N. Fitch, and D. Hausermann, High Press. Res. **14**, 235 (1996).
[16] A. C. Larsen and R. B. Von Dreele, Los Alamos National Laboratory Report No. LAUR 86–748, 2004.
[17] K. Kunc, I. Loa, A. Grzechnik, and K. Syassen, Phys. Status Solidi B **242**, 1857 (2005).
[18] K. Kunc, I. Loa, and K. Syassen, Phys. Rev. B **77**, 094110 (2008).
[19] J. P. Perdew and Y. Wang, Phys. Rev. B **45**, 13244 (1992).
[20] G. Kresse and D. Joubert, Phys. Rev. B **59**, 1758 (1999).
[21] G. Kresse and J. Furthmüller, Phys. Rev. B **54**, 11169 (1996).
[22] H. Monkhorst and J. Pack, Phys. Rev. B **13**, 5188 (1976).
[23] O. H. Nielsen and R. M. Martin, Phys. Rev. B **32**, 3780 (1985).
[24] C. C. Lin and L. G. Liu, Eur. J. Mineral. **9**, 785 (1997).
[25] S. Ono, Phys. Chem. Miner. **34**, 215 (2007).
[26] H. G. von Schnering and N. K. Goh, Naturwiss. **61**, 272 (1974).
[27] I. Kawada, K. Kato, and S. Yamaoka, Acta Crystallogr., Sect. B: Struct. Crystallogr. Cryst. Chem. **32**, 3110 (1976).
[28] M. S. T. Bukowinski, Geophys. Res. Lett. **7**, 689 (1980).
[29] P. Cervantes, Q. Williams, M. Cote, M. Rohlfing, M. L. Cohen, and S. G. Louie, Phys. Rev. B **58**, 9793 (1998).
[30] M. Uludoğan, T. Cagin, A. Strachan, and W. A. Goddard, J. Comput. Aided Mater. Des. **8**, 193 (2002).
[31] S. Drablia, H. Meradji, S. Ghemid, N. Boukhris, B. Bouhafs, and G. Nouet, Mod. Phys. Lett. B **23**, 3065 (2009).
[32] M. Königstein, A. A. Sokol, and C. R. A. Catlow, Phys. Rev. B **60**, 4594 (1999).
[33] P. Vinet, J. R. Smith, J. Ferrante, and J. H. Rose, Phys. Rev. B **35**, 1945 (1987).
[34] K. Haller, J. H. Lunsford, and J. Laane, J. Phys. Chem. **100**, 551 (1996).
[35] D. de Waal, K.-J. Range, M. Königstein, and W. Kiefer, J. Raman Spectrosc. **29**, 109 (1998).

[36] S. T. Weir, Y. K. Vohra, and A. L. Ruoff, Phys. Rev. B **33**, 4221 (1986).
[37] M. Königstein and C. R. A. Catlow, J. Solid State Chem. **140**, 103 (1998).
[38] P. Hohenberg and W. Kohn, Phys. Rev. **136**, B864 (1964).
[39] W. B. Holzapfel, Rep. Prog. Phys. **59**, 29 (1996).
[40] M. T. Yin and M. L. Cohen, Phys. Rev. Lett. **45**, 1004 (1980).
[41] K. Kunc and R. M. Martin, Phys. Rev. B **24**, 2311 (1981).
[42] D. M. Adams and D. Stevens, J. Chem. Soc. Dalton Trans. **1997**, 1097.
[43] D. M. Adams, A. G. Christy, J. Haines, and S. M. Clark, Phys. Rev. B **46**, 11358 (1992).
[44] X. Wang, F. X. Zhang, I. Loa, K. Syassen, M. Hanfland, and Y.-L. Mathis, Phys. Status Solidi B **241**, 3168 (2004).